NANO LETTERS

Letter

pubs.acs.org/NanoLett

Terahertz Generation by Dynamical Photon Drag Effect in Graphene Excited by Femtosecond Optical Pulses

J. Maysonnave,[†] S. Huppert,[†] F. Wang,[†] S. Maero,[†] C. Berger,[‡,§] W. de Heer,[‡] T. B. Norris,[∥] L. A. De Vaulchier,[†] S. Dhillon,[†] J. Tignon,[†] R. Ferreira,[†] and J. Mangeney*[,†]

[†]Laboratoire Pierre Aigrain, Ecole Normale Supérieure, CNRS (UMR 8551), Université P. et M. Curie, Université D. Diderot, 75231 Paris Cedex 05, France

[‡]School of Physics, Georgia Institute of Technology, Atlanta, Georgia 30332, United States

[§]Université Grenoble Alpes/CNRS, Institut Néel, Grenoble, 38042 France

[∥]Center for Ultrafast Optical Science, University of Michigan, Ann Arbor, Michigan 48109-2099, United States

S *Supporting Information*

ABSTRACT: Graphene has been proposed as a particularly attractive material for the achievement of strong optical nonlinearities, in particular generation of terahertz radiation. However, owing to the particular symmetries of the C-lattice, second-order nonlinear effects such as difference-frequency or rectification processes are predicted to vanish in a graphene layer for optical excitations ($\hbar\omega \gg 2E_F$) involving the two relativistic dispersion bands. Here we experimentally demonstrate that graphene excited by femtosecond optical pulses generate a coherent THz radiation ranging from 0.1 to 4 THz via a second-order nonlinear effect. We fully interpret its characteristics with a model describing the electron and hole states beyond the usual massless relativistic scheme. This second-order nonlinear effect is dynamical photon drag, which relies on the transfer of light momentum to the carriers by the ponderomotive electric and magnetic forces. The model highlights the key roles of next-C-neighbor couplings and of unequal electron and hole lifetimes in the observed second-order response. Finally, our results indicate that dynamical photon drag effect in graphene can provide emission up to 60 THz, opening new routes for the generation of ultrabroadband terahertz pulses.

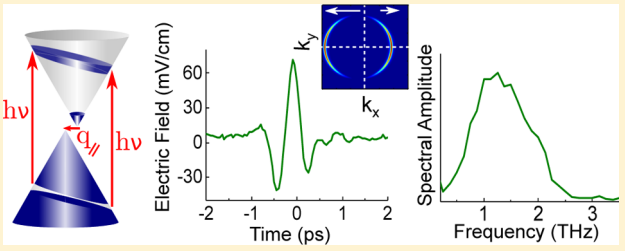

KEYWORDS: *Graphene, terahertz, photon drag, optical rectification, second-order nonlinearity, next-nearest-neighbor*

Current terahertz (THz) technologies suffer from the lack of compact room temperature THz sources, limiting the proliferation of consumer applications. As a consequence, an important activity in this field is dedicated to developing sources such as photoconductive devices,[1,2] quantum cascade lasers,[3] or exploring new schemes for THz generation-like intracavity difference-frequency generation in mid-infrared quantum cascade lasers.[4] In parallel, an important effort is dedicated to the study of new physical properties within novel materials.[5,6] Owing to its gapless electronic band structure, graphene is gaining increasing attention for new developments in the THz domain.[7] In addition, graphene exhibits a large nonlinear optical response arising from the linear carrier energy dispersion, together with the high electron velocity near the Dirac point.[8] Harmonic generation at THz frequencies relying on a third-order nonlinearity has been recently demonstrated in graphene using a femtosecond optical excitation at normal incidence.[9] Although second-order nonlinear effects such as difference-frequency or rectification processes are generally considerably stronger and therefore of importance in applications; these are forbidden by symmetry as graphene is a centrosymmetric material. Second-order nonlinearities only appear when the photoexcited medium possesses an anisotropy axis, which imposes a preferential direction of motion for the carriers. However, the photoexcitation can itself introduce an anisotropy direction, related to the in-plane photon momentum $\vec{q}_{//}$. Indeed, second-order nonlinear *dc*-currents involving only conduction electrons have recently been demonstrated in graphene, under monochromatic photoexcitation at oblique incidence and at energy $\hbar\omega < E_F$.[10,11] Recent experiments on graphene excited by femtosecond optical pulses at photon energy $\hbar\omega \gg 2E_F$ at oblique incidence have shown second-order nonlinear *ac*-currents associated with narrowband THz generation at room temperature.[12]

In this work, we demonstrate that the dynamical photon drag effect in graphene excited by femtosecond optical pulses ($\hbar\omega \gg 2E_F$) generates broadband, and potentially ultrabroadband THz radiation, and present a microscopic model that fully describes the emission characteristics. This dynamical photon drag effect results from the transfer of light momentum to the photogenerated electron and hole distributions by the ponderomotive electric and magnetic forces. We show, by

Received: July 15, 2014
Revised: September 4, 2014
Published: September 16, 2014

   dx.doi.org/10.1021/nl502684j | *Nano Lett.* 2014, 14, 5797−5802

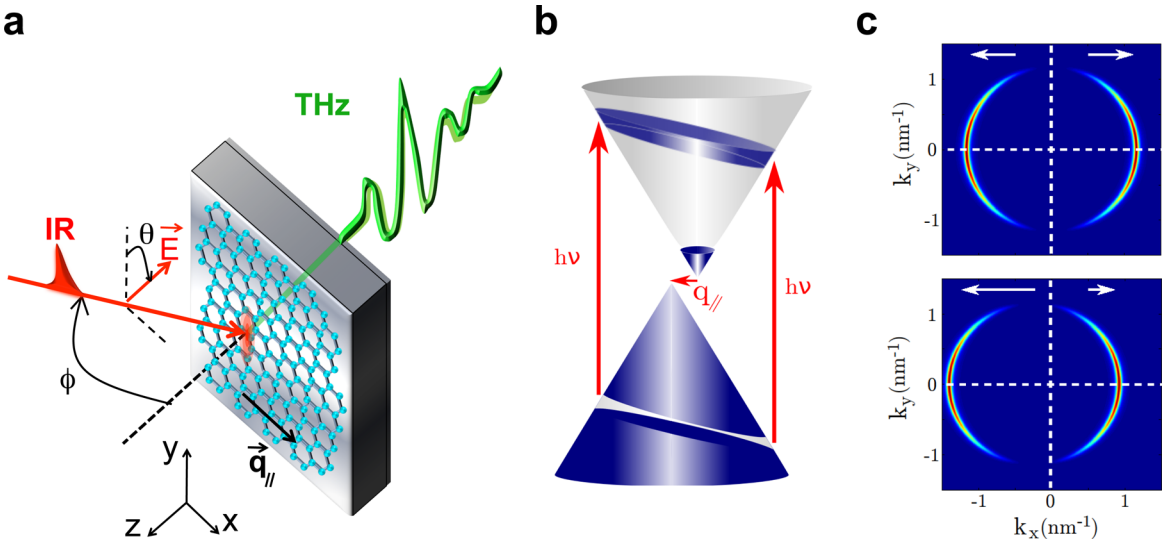

Figure 1. Dynamical photon drag effect resulting from the dynamical transfer of light momentum to the photogenerated electron and hole distributions. (a) A femtosecond optical pump pulse illuminates the multilayer graphene and creates nonequilibrium electron and hole populations. A transient photon drag current is then generated in the plane of the graphene sheets, which emits a THz pulse. The THz pulse is transmitted through the SiC substrate, collected by an off-axis parabolic mirror and detected in the time-domain using electro-optic sampling in a 1-mm-thick ZnTe crystal. (b) Transient nonthermal electron and hole distributions in the interband regime for an oblique illumination; the electron and hole population distributions are not symmetric with the respect to the center of the Dirac cone. (c) Nonequilibrium electron population distribution generated by p-polarized femtosecond optical pulses at normal incidence (upper panel) and at oblique incidence (lower panel). The photon momentum was artificially enhanced by a factor 100 in this simulation to make clear the displacement relative to the center of the Dirac cone. The white arrows represent the integrated momentum of the two population distribution lobes. Whereas at normal incidence, the two contributions to the current compensate perfectly, this is not the case at oblique incidence, where a net current is generated. This current changes in direction and amplitude with the direction of the exciting optical electric field, as the latter determines the position of the population distribution lobes around the Dirac cone.

experimental investigations and theoretical modeling, that this second-order nonlinear process relies on the intrinsic asymmetry between the conduction and the valence bands (i.e., different energy dispersions and lifetimes) and consequently is described by electron and hole states beyond the usual massless relativistic scheme. Interestingly, our findings provide a direct probe of the next-nearest-neighbor couplings[13] in graphene that have been difficult to access by experiments[14] and are known to induce nontrivial effects in graphene.[15]

The investigated multilayer graphene sample is produced by thermal desorption of Si from the C-terminated face of single-crystal 4H-SiC(0001) and contains typically 35−40 layers with non-Bernal rotated graphene planes.[16] It has been shown that each graphene sheet possesses a band structure very similar to that of an individual graphene monolayer[17] and that the first four layers near the substrate are heavily doped, whereas the upper remaining layers are quasi-neutral ($E_F \sim 8$ meV). The experiment, illustrated in Figure 1a, uses a mode-locked Ti:Sa laser delivering 110 fs optical pulses at a repetition rate of 80 MHz with an optical fluence ranging up to 35 μJ/cm^2. It consists of optical pump pulses that excite the graphene sample, generating transient nonthermal electron and hole distributions in the interband regime. As shown on upper panel of Figure 1b, for normal incidence of the optical excitation, the nonthermal electron and hole population distributions are symmetric with the respect to the center of the Dirac cone, whereas for an oblique illumination, the two population distributions are not symmetric (lower panel of Figure 1b and c). Consequently, at oblique incidence, a net transient current is generated and THz radiation is emitted from the graphene sample. This THz radiation is coherently detected by optical probe pulses using conventional electro-optic detection techniques.[18] The central wavelength of the optical pump pulses is 800 nm corresponding to $\hbar\omega = 1.55$ eV $\gg 2E_F$. The graphene sample is placed at the focal plane of an aspherical optical lens (effective focal length of 50 mm), so that the incidence angle ϕ of the optical excitation (see Figure 1a) can be varied by displacing the pump beam position on the surface of the lens. Since the electro-optic detection technique is only sensitive to synchronized THz radiation with femtosecond pulses, the incoherent thermal background is suppressed.[19] All measurements are performed at room temperature.

The THz waveform $\vec{E}_{THz}(t)$ generated by exciting the graphene sample with an angle $\phi = 25°$ is reported in Figure 2a. For this measurement, the pump excitation is s-polarized ($\theta = 0$ in Figure 1a), and the electro-optic sampling detection setup is oriented to detect the projection of $\vec{E}_{THz}(t)$ along the x-axis (see Figure 1a). In this configuration, we experimentally verified that, in agreement with theory,[20] second-order nonlinear effects in the SiC substrate are canceled (see Supporting Information). The observed THz waveform shows a main positive peak with a full-width-at-half-maximum of 230 fs, followed by oscillations at longer times. As shown below, these oscillations are induced by the limited bandwidth of the electro-optic detection system.[21] The amplitude spectrum, obtained by the Fourier transform of the temporal electric field waveform, consists of a single broad peak centered at 1.25 THz, as shown in Figure 2b.

Figure 2e shows that the amplitude of $\vec{E}_{THz}(t)$ scales linearly with the excitation fluence and thus quadratically with the incident optical electric field, indicating a second-order nonlinear process. The shape of the electro-optic waveform remains essentially constant for all incident fluences. The electric field peak amplitude reaches 70 mV/cm at an optical

dx.doi.org/10.1021/nl502684j | Nano Lett. 2014, 14, 5797−5802

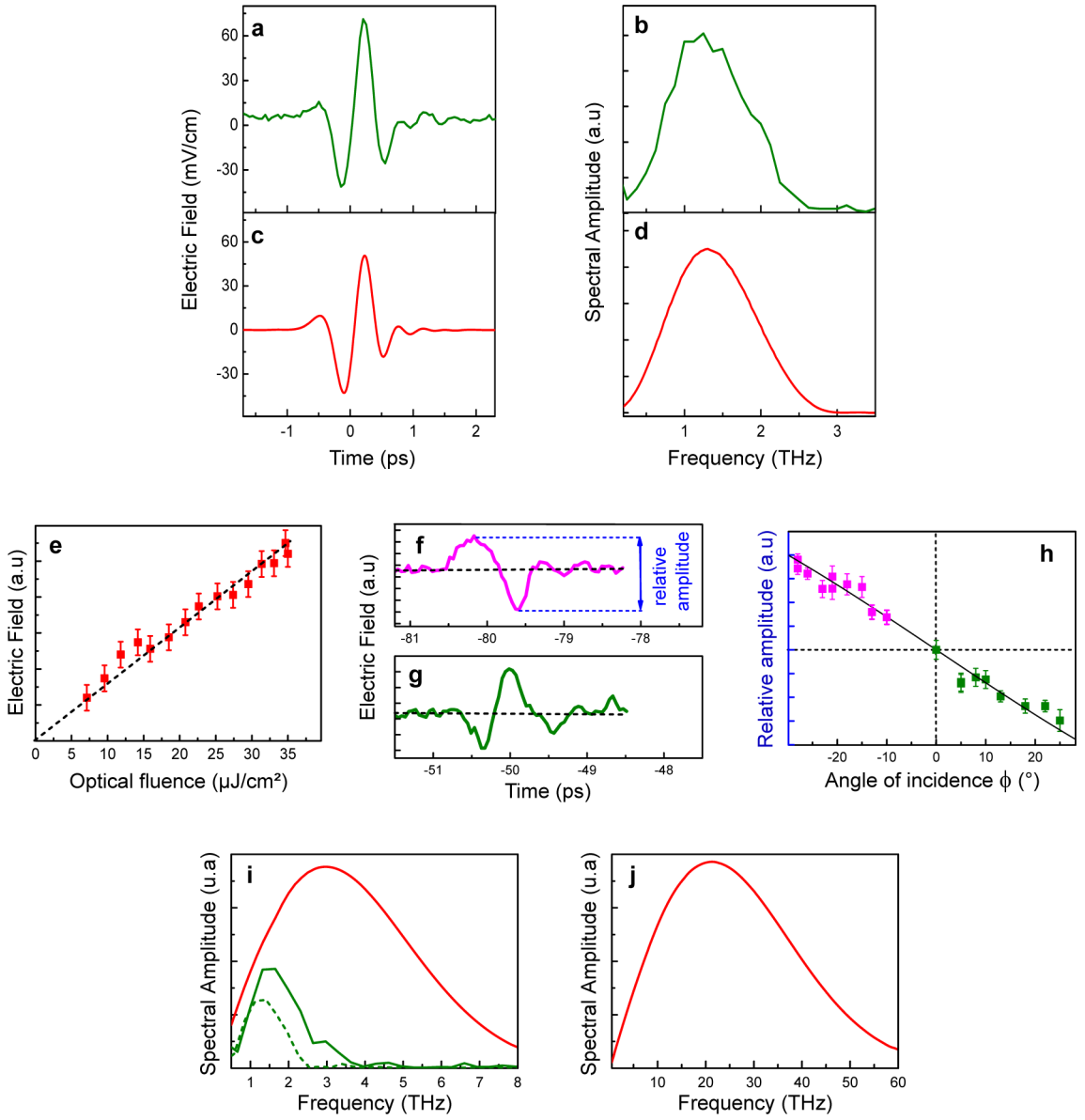

Figure 2. Measured and calculated THz electric field emitted by multilayer graphene. (a) Experimental electric field waveform emitted by the multilayer graphene illuminated by s-polarized femtosecond optical pulses at 800 nm central wavelength under an incidence angle $\phi = 25°$ and its associated spectrum (b). (c) Calculated electric field waveform emitted by the multilayer graphene excited in similar conditions as in (a) and its associated spectrum (d). (e) THz electric field amplitude as a function of the optical fluence incident on the multilayer graphene. The red squares are the experimental data, and the error bars show the standard deviation associated with noise fluctuations. The dashed line underlines the linear dependence. (f–g) Time-resolved electric field profiles measured for two opposite angles of incidence ($\phi = \pm 14°$) under s-polarized optical excitation. (h) The peak-to-peak amplitude of emitted THz electric field normalized by $(1 - r)$, with r the amplitude Fresnel coefficient of graphene, as a function of the incidence angle of the femtosecond optical pulses ϕ. The squares are the experimental data, the error bars show the standard deviation associated with noise fluctuations, and the black solid line is the best-fit sinus curve. (i) Amplitude spectra of the THz electric field emitted by graphene excited by 110 fs optical pulses measured with a 1-mm-thick ZnTe crystal (green dashed curve), with a 200-μm-thick ZnTe crystal (green solid curve) and calculated without any convolution with the experimental setup response (red curve). (j) Calculated amplitude spectrum of the THz signal emitted by graphene excited by 15 fs optical pulses.

fluence of 35 μJ/cm^2, corresponding to an optical-to-THz conversion efficiency of 1.5×10^{-11}. Such a value is moderate, but the graphene sample is extremely thin (~14 nm) and the conversion efficiency par length unit reaches $\sim 10^{-5}$/cm. In order to probe the role of the in-plane photon momentum in the THz generation process, $\vec{E}_{\mathrm{THz}}(t)$ is measured for different incidence angles ϕ under s-polarization. In contrast with usual second-order nonlinear processes in two-dimensional systems under s-polarized excitation that are insensitive to the incidence angle, we observe critical changes in the emitted electric field waveform as a function of ϕ. At normal incidence ($\phi = 0$) no THz signal is detected. For opposite incidence angles, the time-oscillations show reverse polarity, as shown in Figure 2f and g for $\phi = \pm 14°$. These results are summarized in Figure 2h, which shows that the relative field amplitude is proportional to the incident angle and therefore to the in-plane component of the photon momentum. This is a distinctive feature of the dynamical photon drag effect, i.e., the transfer of light momentum to the photogenerated electron and hole distributions by the transient ponderomotive electric and

dx.doi.org/10.1021/nl502684j | Nano Lett. 2014, 14, 5797–5802

magnetic forces. Note that the shape of the waveforms remains essentially unchanged for all incident angles. We show in Figure 2i that, by using a less sensitive but more broadband ZnTe crystal (200 μm thick), the amplitude spectrum is shifted to higher frequencies with detected components up to 4 THz. This observation indicates that the spectral content of the measured THz radiation is limited by the experimental setup response.

In order to describe quantitatively the experimental findings and interpret the temporal waveform of the THz signal, we have calculated the time-dependent average current $\langle \vec{j} \rangle$ generated in one graphene layer excited by femtosecond optical pulses, up to the second order in the exciting electric field: $\vec{E}(\vec{r},t) = \mathrm{Re}[E_0 \exp(i\vec{q}\cdot\vec{r} - i\omega t)] \exp(-t^2/2\tau^2)\vec{\varepsilon}$ with τ the 1/e width of the laser pulses (τ = 110 fs). To this end, we calculated the density matrix evolution in the standard perturbation formalism: $i\hbar\, \partial\rho^{(n)}/\partial t = [H_0,\rho^{(n)}] + [V_{\mathrm{dip}},\rho^{(n-1)}] - i\hbar\, \Gamma_n \rho^{(n)}$ up to the second order (n = 1,2) in the dipolar perturbation $V_{\mathrm{dip}} = e\vec{A}\cdot\vec{p}/m_0$. Γ_n are phenomenological dampings. In the basis of the graphene eigenstates $|\xi,\lambda,\vec{k}\rangle$ (where ξ is the Dirac-valley index, λ the band label, and k the in-plane wavevector), $\rho^{(0)}$ is purely diagonal and reflects the thermal electron distribution at room temperature before the optical pulse excitation. The THz radiation emitted in the far field is obtained as the time-derivative of the second-order current: $\vec{E}_{\mathrm{THz}}(t) \propto \partial \mathrm{Tr}[\vec{p}\rho^{(2)}]/\partial t$. The dominant terms in the calculation of $\vec{E}_{\mathrm{THz}}(t)$ involve only the diagonal elements of $\rho^{(2)}$, i.e., the transient electron and hole nonlinear populations generated by the laser pulse. These transient populations display oscillations at the frequency differences between the various spectral components of the exciting pulse, characterizing thereby a q-dependent optical rectification process. Figure 1b schematically shows the anisotropic electron population distribution in the momentum space at the pulse maximum for a s-polarized exciting optical pulse, calculated in the usual nearest-neighbor (NN) tight-binding approximation and taking a band-independent damping Γ_2. At normal incidence (Figure 1b, upper panel), currents from electrons with opposite wavevectors cancel each other. At oblique incidence, however (Figure 1b, lower panel), the population distribution is displaced relatively to the center of the Dirac cone, and a net conduction current appears. Nonetheless, the valence current has an opposite direction and compensates exactly the conduction current. Consequently, the total transient current $\langle \vec{j} \rangle$ vanishes for excitation between the valence and conduction massless relativistic dispersion bands. We thus consider the electron and hole states beyond the usual relativistic scheme and account for the next-nearest-neighbor (NNN) coupling. The inclusion of the NNN coupling in the tight-binding model breaks the mirror symmetry between conduction and valence bands: to the lowest order in **k**, this adds a positive quadratic term to both dispersions, increasing the electron velocity and reducing the hole one. As a consequence, a net second-order current arises. To be consistent, the model also includes the possibility for the damping coefficients Γ_2^{e} and Γ_2^{h} for electrons and holes to be different. There are thus two electron−hole asymmetry sources in the model. It turns out that both of them contribute to the dynamical photon drag current, as discussed below. The following tight binding parameters have been used: the NN (NNN) energy hopping t = 3 eV (t' = 0.15 eV) and an overlap between NN orbitals of s = 0.1. The best overall agreement with the experiments was found for $1/\Gamma_2^{\mathrm{e}}$ = 170 fs and $1/\Gamma_2^{\mathrm{h}} = 1.025/\Gamma_2^{\mathrm{e}}$. Once these quantities are fixed, we convolute the calculated $\vec{E}_{\mathrm{THz}}(t)$ with the experimental setup response function, which is a high-frequency filter with a cutoff at ∼3THz. The complete model becomes thus predictive and, as we show in the following, allows a quantitative analysis of the various dependencies of the measured THz emission: the incidence angle ϕ, the optical polarization θ, and the THz polarization in the x- or y-directions. Note finally that the model naturally incorporates the contributions of ponderomotive forces of both electric and magnetic origins to the interband momentum transfer: in this workframe, the THz emission results from the different accelerations and dampings of photogenerated holes and electrons distributions by the intense excitation fields.

We show in Figure 2c the calculated transient signal $\vec{E}_{\mathrm{THz}}//\vec{x}$ for ϕ = 25° and θ = 0°. It is in very good agreement with the measured waveform (Figure 2a), and importantly, its amplitude is consistent with the experimental value. Moreover, the dynamical photon drag model nicely reproduces the experimental features in Figure 2e to h: the signature of a second order effect with its dependence on input power and the linear variation of $\vec{E}_{\mathrm{THz}}$ with $\vec{q}_{//}$. The broadband nature of the photon drag signal is highlighted in Figure 2i, which reports the calculated amplitude spectra of the THz electric field emitted by graphene without any convolution with experimental setup response: spectral components up to 9 THz are emitted in the far-field region. Moreover, Figure 2j shows the calculated amplitude spectra for an ultrashort optical excitation of 15 fs duration, providing ultrabroadband coherent emission up to 60 THz.

The model can be further tested probing the dependencies with the polarizations of the incoming optical and outgoing THz radiations as reported in Figure 3. When θ is varied, the anisotropic population distributions $\rho^{(2)}(\vec{k},t)$ rotate correspondingly in the **k**-plane, strongly changing the amplitude and direction of the photon drag current, and therefore of the emitted field $\vec{E}_{\mathrm{THz}}(t)$. The dynamical photon drag effect in graphene has a strong signature for two symmetric polarizations relative to p or s directions (e.g., θ = 45° and θ = 135°): the temporal profiles are identical for THz electric fields along the x-direction (Figure 3a) and opposite for the y-direction (Figure 3c). We experimentally confirm this behavior in Figure 3a and c that report the measured THz signals along the x- and the y-directions, respectively, at the specific polarization angles of θ = 45° and θ = 135°. Such an agreement also appears when we compare the Fourier transform $\vec{E}_{\mathrm{THz}}(\nu_{\mathrm{THz}})$ of the detected THz signal, as shown in the Figure 2b and d and Figure 3e and f. Note that under p-polarized optical excitation, a second-order nonlinear effect in SiC substrate contributes to the THz emission for only 30% of its amplitude and at low frequency (<2 THz) as shown in the Supporting Information. In addition, the agreement between the measurements and the monolayer model is less accurate when the z-component of the exciting field becomes significant. In particular, a nonvanishing THz field is measured along the y direction in the p configuration, although it is symmetry-forbidden in monolayer graphene. We attribute these discrepancies observed only for p-polarization to stacking effects that break graphene symmetry[22] and should be further investigated in a future work. We stress that in Figure 3e and f the peak frequency of the THz signal emitted along the x direction is higher for the p than for s excitation configuration. Strikingly, both electron−hole asymmetry sources (NNN contribution and different damping coefficients) are needed to reproduce this spectral feature. Moreover, the analysis of this

dx.doi.org/10.1021/nl502684j | Nano Lett. 2014, 14, 5797−5802

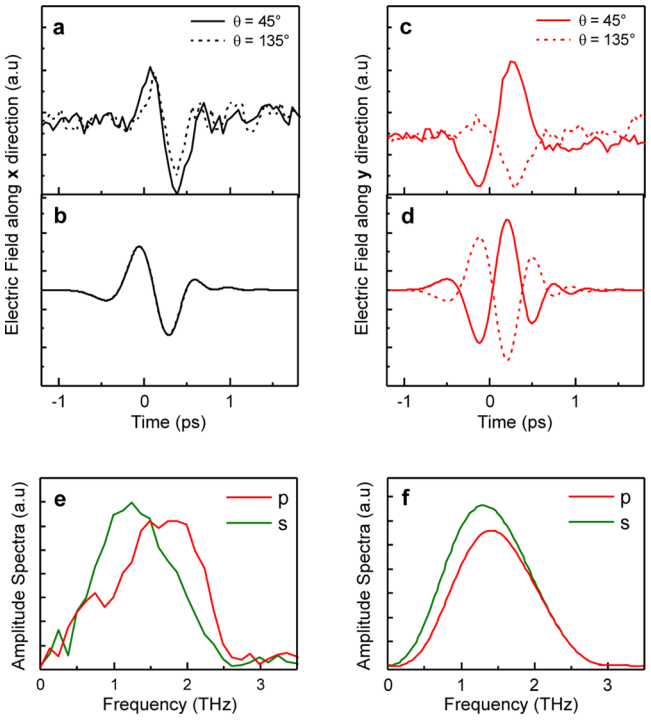

Figure 3. Evolution of the THz electric field with the orientation of the linear polarization of the optical pulses. Measured (a) and calculated (b) electric field waveforms emitted by the multilayer graphene excited by linearly polarized optical pulses and detected in the *x*-direction for two different orientations of the optical polarization $\theta = 45°$ (solid line) and $\theta = 135°$ (dashed line). Measured (c) and calculated (d) electric field waveforms emitted by multilayer graphene excited by linearly polarized optical pulses and detected in the *y*-direction for two different orientations of the optical polarization $\theta = 45°$ (solid line) and $\theta = 135°$ (dashed line). Spectra of the experimental (e) and calculated (f) transient electric field emitted by multilayer graphene illuminated by s-polarized (green) and p-polarized (red) femtosecond optical pulses and detected in the *x*-direction.

frequency shift in the framework of our model permits to extract useful information on the carrier's relaxation processes. Indeed, the computed signal exhibits shift to higher frequency from s- to p-polarization only if the hole scattering time is taken larger than the electron one. For the moderate optical fluence used in this study (<40 μJ/cm^2), the involved relaxation rates Γ_2^e and Γ_2^h are mainly related to carrier-phonon scattering, which efficiently randomizes the direction of carrier wavevector,[23,24] making the current vanish.

Our experimental and theoretical study pinpoints the essential physical aspects underlying the dynamical photon drag effect in graphene excited by femtosecond optical pulses with a photon energy much higher than the Fermi level energy. Moreover, it offers a unique probe of physical properties of graphene such as the next-nearest-neighbor coupling and the distinct dynamics of nonthermal electron and hole population that are otherwise difficult to evaluate. The consideration of the next-nearest-neighbor coupling in the theoretical predictions is in contrast to most optical processes in graphene for which this coupling provides only small corrections to the modeling. Here, this coupling, as well as the asymmetry between the electrons and holes dynamics, is intrinsically related to the observed phenomena. Moreover, the new insights provided by our study in the dynamics of the nonequilibrium electron and hole populations during the first hundred of femtoseconds after interband excitation are particularly fascinating since optical gain and population inversion in graphene are possible only in this time window.[25] Furthermore, our work has important implications for THz technology since these results demonstrate that a dynamical photon drag effect in multilayer graphene provides an original scheme for coherent pulsed THz emission. Our results pave the way to exploit dynamical photon drag effects in many other materials such as graphene-like materials or carbon-based materials.

■ ASSOCIATED CONTENT

Supporting Information

THz emission from bare SiC substrate and comparison with THz emission from multilayer graphene with its SiC substrate. This material is available free of charge via the Internet at http://pubs.acs.org.

■ AUTHOR INFORMATION

Corresponding Author

*E-mail: juliette.mangeney@lpa.ens.fr (phone: +33(1) 44323507). Address: Laboratoire Pierre Aigrain, Ecole Normale Supérierue, 24 rue Lhomond, 75005 Paris cedex, France.

Notes

The authors declare no competing financial interest.

■ REFERENCES

(1) Berry, C. W.; Wang, N.; Hashemi, M. R.; Unlu, M.; Jarrahi, M. Significant performance enhancement in photoconductive terahertz optoelectronics by incorporating plasmonic contact electrodes. *Nat. Commun.* **2013**, *4*, 1622.

(2) Peytavit, E.; et al. Milliwatt-level output power in the sub-terahertz range generated by photomixing in a GaAs photoconductor. *Appl. Phys. Lett.* **2011**, *99*, 223508.

(3) Brandstetter, M.; et al. High power terahertz quantum cascade lasers with symmetric wafer bonded active regions. *Appl. Phys. Lett.* **2013**, *103*, 171113.

(4) Lu, Q. Y.; Bandyopadhyay, N.; Slivken, S.; Bai, Y.; Razeghi, M. Room temperature terahertz quantum cascade laser sources with 215 μW output power through epilayer-down mounting. *Appl. Phys. Lett.* **2013**, *103*, 011101.

(5) Liao, L.; Bai, J.; Cheng, R.; Lin, Y.; Jiang, S.; Qu, Y.; Huang, Y.; Duan, X. Sub-100 nm Channel Length Graphene Transistors. *Nano Lett.* **2010**, *10*, 3952−3956.

(6) Nevou, L.; Giraud, E.; Castellano, F.; Grandjean, N.; Faist, J. Interaction between meta-materials and shallow donors in bulk GaN at THz frequency. *Opt. Exp.* **2014**, *22*, 3199−3207.

(7) Low, T.; et al. Graphene Plasmonics for Terahertz to Mid-Infrared Applications. *ACS Nano* **2014**, *8*, 1086−1101.

(8) Glazov, M. M.; Ganichev, S. D. High frequency electric field induced nonlinear effects in graphene. *Phys. Rep.* **2014**, *535*, 101−138.

(9) Sun, D.; et al. Coherent Control of Ballistic Photocurrents in Multilayer Epitaxial Graphene Using Quantum Interference. *Nano Lett.* **2010**, *10*, 1293−1296.

(10) Karch, J.; et al. Dynamic Hall effect driven by circularly polarized light in a graphene layer. *Phys. Rev. Lett.* **2010**, *105*, 227402.

(11) Jiang, C.; et al. Helicity-dependent photocurrents in graphene layers excited by midinfrared radiation of a CO_2 laser. *Phys. Rev. B* **2011**, *84*, 125429−39.

(12) Obraztsov, P. A.; et al. All-optical control of ultrafast photocurrents in unbiased graphene. *Sci. Rep.* **2014**, *4*, No. 4007.

(13) Kadirko, V.; Ziegler, K.; Kogan, E. Next-Nearest-Neighbor Tight-Binding Model of Plasmons in Graphene. *Graphene* **2013**, *2*, 97−101.

(14) Kretinin, A.; et al. Quantum capacitance measurements of electron-hole asymmetry and next-nearest-neighbor hopping in graphene. *Phys. Rev. B* **2013**, *88*, 165427.

(15) Peres, N. M. R.; Guinea, F.; Castro Neto, A. H. Electronic properties of disordered two-dimensional carbon. *Phys. Rev. B* **2006**, *73*, 125411.
(16) De Heer, W.; et al. Large area and structured epitaxial graphene produced by confinement controlled sublimation of silicon carbide. *Proc. Natl. Acad. Sci. U.S.A.* **2011**, *108*, 16900.
(17) Sprinkle, M.; et al. First direct observation of a nearly ideal graphene structure. *Phys. Rev. Lett.* **2009**, *103*, 226803.
(18) Lee, Y. S. *Principles of THz Science and Technology*; Springer: New York, 2009; Ch. 3.
(19) Chen, Q.; Tani, M.; Jiang, Z.; Zhang, X.-C. Electro-optic transceivers for terahertz-wave applications. *J. Opt. Soc. Am. B* **2001**, *18*, 823−831.
(20) Strait, J. H.; et al. Emission of terahertz radiation from SiC. *Appl. Phys. Lett.* **2009**, *95*, 051912.
(21) Bakker, H. J.; Cho, G. C.; Kurz, H.; Wu, Q. Distortion of terahertz pulses in electro-optic sampling. *J. Opt. Soc. Am. B* **1998**, *15*, 1795.
(22) Sprinkle, M.; et al. Multilayer epitaxial graphene grown on the SiC (0001) surface; structure and electronic properties. *J. Phys. D: Appl. Phys.* **2010**, *43*, 374006.
(23) Sun, D.; et al. Current Relaxation due to Hot Carrier Scattering in Graphene. *New J. Phys.* **2012**, *14*, 105012.
(24) Malic, E.; Winzer, T.; Knorr, K. Efficient orientational carrier relaxation in optically excited graphene. *Appl. Phys. Lett.* **2012**, *101*, 213110.
(25) Gierz, I.; et al. Snapshots of non-equilibrium Dirac carrier distributions in graphene. *Nat. Mater.* **2013**, *12*, 1119−1124.